Metrical properties of a collection of 2D parallel thinning algorithms

Antoine Manzanera, Thierry Bernard

Metrical properties of a collection of 2D parallel thinning algorithms

Antoine Manzanera *

Ecole Nat. Sup. de Techniques Avancées, 32 Bd Victor, 75015 Paris - FRANCE

Thierry M.Bernard

Ecole Nat. Sup. de Techniques Avancées, 32 Bd Victor, 75015 Paris - FRANCE

Abstract

This paper is dedicated to the study of metrical properties of a collection of 2D thinning algorithms that we have proposed. Here, we characterize their underlying metrics and use it to reduce the classical metrical biases that affect thinning algorithms in the square grid. We show that some algorithms from the collection lead to skeletons based on a particular geometry, corresponding to the (4,8)-median axis, which is a new shape descriptor, featuring nice robustness and conditioning properties.

Key words: digital geometry, parallel thinning algorithm, (4,8)-median axis

1 Introduction

We have recently proposed a family of 2-dimensional thinning algorithms to compute the skeleton of binary discrete images. We systematically constructed them from the discretization of the evolution equation of a monotonous propagating front, under topology preservation constraints, in the different connectivity models of the square grid, and for different parallelization schemes. Logic minimization was an important issue in their genesis. The eight algorithms, referred to as MB, are summarized on Figure 1, with a comparison of their different properties. The name of every algorithm is given according to

* corresponding author
Email address: manzaner@ensta.fr (Antoine Manzanera).
URL: http://www.ensta.fr/~manzaner (Antoine Manzanera).

the three binary labels: (1) *-fp* or *-dir* for fully parallel or directional, (2) -1 or -2 depending on the number of directions of propagation (4 or 8 respectively), and (3) -4 or -8 depending on the topology. The Boolean definition of every algorithm is presented on Figure 1: the principle of the algorithms is to delete iteratively all pixels matching the removing condition, provided that they do not match the non removing condition. For the fully parallel algorithms, all patterns are to be considered with their $\pi/2$ rotated versions. For the MBfpx-4 algorithms (x = 1 or 2), a special convention is used: the white pixels with a red dot (resp. black pixels with a green square) are the black pixels of the original image matching (resp. not matching) the removing condition. The derivation, proof, and details of implementation of each one of these algorithms can be found in [8]. Note that MBfp1-8 is equivalent to the algorithm proposed in [3], and MBfp1-4 is equivalent to the algorithm proposed in [6]. Figure 1 synthesizes some combinatorial (e.g. Boolean complexity and support) and topological (e.g. P-simpleness [1]) properties that are not addressed in this paper, but detailed in [8].

The aim of this paper is to study the metrical properties of these algorithms.

ALGORITHM	Removing condition	Non–removing condition	Parallelism	Topology preservation	Isotropy	1–pixel thickness	Boolean complexity	Support and size	P–simpleness
MBdir1–8			DIR	8	NO	YES	28 r	8 (8)	YES
MBdir2–8			DIR	8	NO	YES	76 r	 8 (8)	YES
MBdir1–4			DIR	4	NO	YES	28 r	 7 (8)	YES
MBdir2–4			DIR	4	NO	YES	60 r	 7 (8)	YES
MBfp1–8 [Eckhardt et al. 93]			FP	8	YES	NO	18 ρ	 13	YES
MBfp2–8	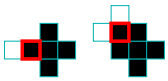		FP	8	YES	NO	28 ρ	 21	YES
MBfp1–4 [Latecki et al. 95]			FP	4	NO	NO	16 ρ	 23	YES
MBfp2–4	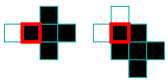		FP	4	NO	NO	26 ρ	 38	NO

Fig. 1. The MB family of parallel thinning algorithms.

In Section 2, we show that the geometry of the MB skeletons can be formally characterized by the type of median axis that they each contain. In particular, the (4,8)-median axis is defined as the mixed case of a generic median axis including the classical morphological skeletons for the two canonical distances of the square grid. We show that the (4,8)-median axis is the locus of the cen-

ters of the maximal elements from a collection of sets called (4,8)-fuzzy balls, which are formally defined. In Section 3, we show how the different underlying metrics of the algorithms lead to different behaviors with respect to rotation invariance and noise immunity, and discuss the issue of approximating Euclidean skeletons with thinning algorithms in the square grid.
Conclusions and perspective work are presented in Section 4.

2 (K-P)-median axis and metrical properties of MB

As shape descriptor, it is obvious that the metrical properties of a skeleton are very important ; the initial shape must be recovered at least approximately from its weighted skeleton, slight variations on the contour should not lead to significant changes in the skeleton, and the skeleton must be fairly invariant to arbitrary rotations or scalings. Nevertheless, these issues are rather poorly addressed by the thinning approaches. There are other skeletonization methods designed in Euclidean frameworks, either continuous [9] or discrete [4], that address explicitly the metrical issues, at the price of a representation change, implying a higher computational cost and a loss of regularity.

We wish to give in this paper a formal description of the metrical behavior of the proposed thinning algorithms, whose results can be seen on Figure 2. The geometry of the skeletons are based on different median axis, depending on the type of parallelism and the directions of deletion. We now recall the formalism needed to introduce our generic median axis:
The discrete plane is mapped to the *square grid* $\mathbb{Z}^2$, a (binary) *image* X is a subset of $\mathbb{Z}^2$. A *pixel* x is an element of $\mathbb{Z}^2$. The two canonical discrete distances of the square grid are respectively the *4-distance* d_4, and the *8-distance* d_8. If $x = (x_1, x_2)$ and $y = (y_1, y_2)$, then $d_4(x, y) = |x_1 - y_1| + |x_2 - y_2|$ and $d_8(x, y) = \max(|x_1 - y_1|, |x_2 - y_2|)$.
The (K, P)-*median axis* of image X (K and P are equal to 4 or 8 and $K \leq P$) is defined as:

$$S_K^P(X) = \bigcup\{x \in X; (y \in X \text{ and } d_P(x, y) = 1) \Rightarrow d_K(x, X^c) \geq d_K(y, X^c)\}$$

So the (K, P)-median axis is the set of the maxima of distance d_K, in the P-neighborhood. Depending on the values of K and P, this leads to three different median axes, shown on row 1 of Figure 2. We are going to show that these different median axes determine the metrical properties of the different algorithms.

As every iteration (resp. four successive sub-iterations) of MBfp (resp. MBdir) examines the 4-contour (resp. the 8-contour), the geometry of the resulting skeleton is based on distance d_4 (resp. d_8), as it can be seen on Figure 2. In the case of the MBfp 8-connected algorithms, the isotropy allows even to prove

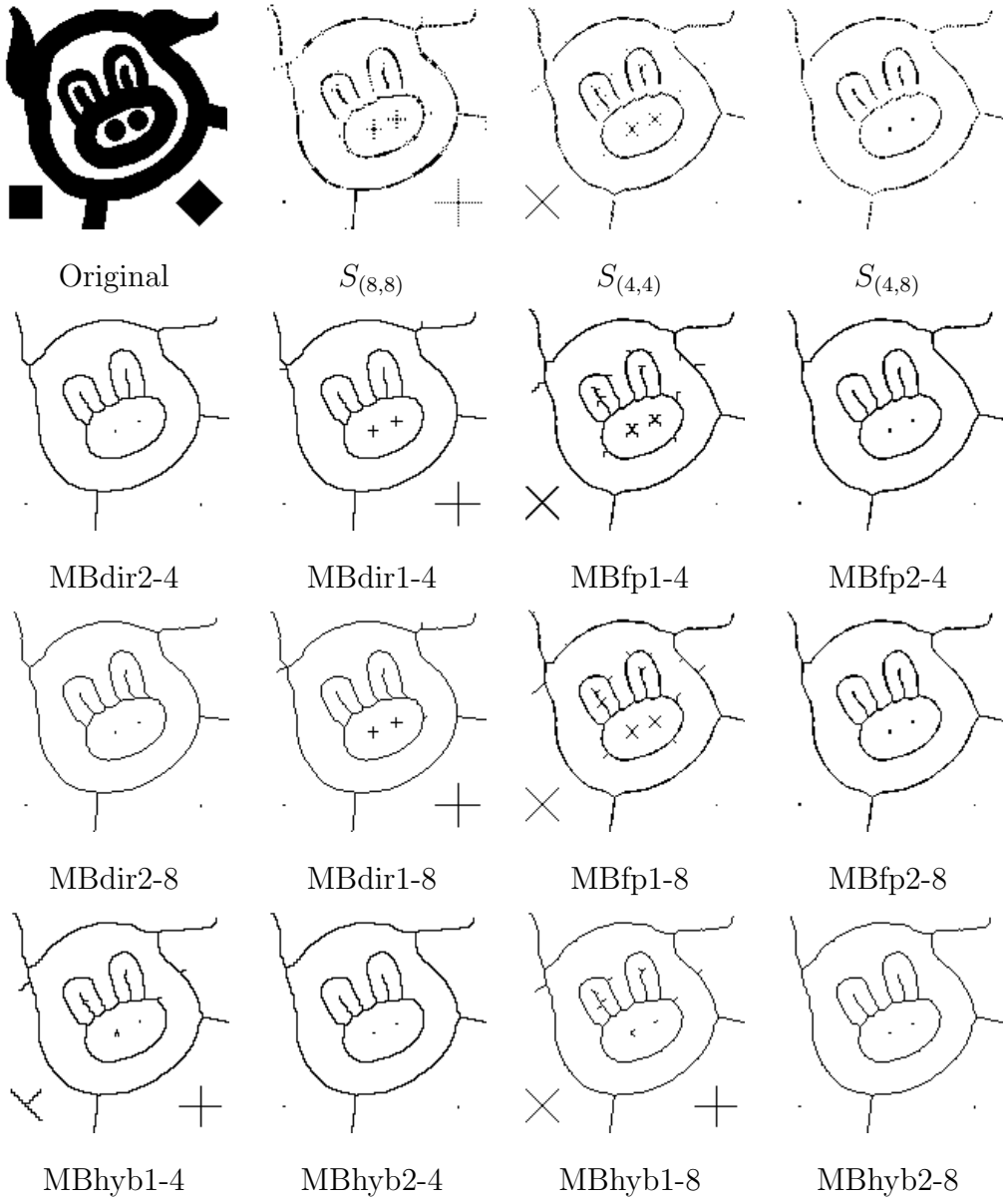

Fig. 2. Metrical properties of the MB skeletons.

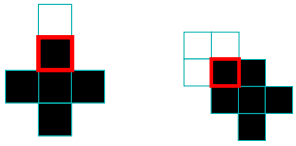

Fig. 3. Deletion patterns of the MBfp- skeletons.

formally that, if the pixels are examined in the order induced by the distance d_4 to the border, then:

(1) $S_4^4(X) \subset$ MBfp1-8(X) and (2) $S_4^8(X) \subset$ MBfp2-8(X).

Indeed, if a pixel p matches pattern (α_1) (resp. (α_1) or (α_2)) shown on Figure 3 (or one of their $\pi/2$ rotated versions), then it is 4−adjacent (resp. 8−adjacent) to a 4-interior point q, such that $d_4(q, X^c) = d_4(p, X^c)+1$, so $p \notin S_4^4(X)$ (resp. $p \notin S_4^8(X)$). These properties are verified for most images, because except in pathological cases (some examples can be seen in [7]), the MBfp thinning respect the order induced by distance d_4. It follows that the geometry of the each MB-skeleton is determined by the geometry of the corresponding (K, P)-*median axis*. We are now going to characterize the geometry of the $(4, 8)$-*median axis*, thanks to the notion of $(4, 8)$-*fuzzy balls*, that we define further:
For $K = 4$ or 8, the *K-ball* of center x and radius n is defined as $B_K(x, n) = \{z \in \mathbb{Z}^2, d_K(x, z) \leq n\}$. A ball $B_K(x, n)$ is said to be *maximal* in the image X if $\forall (y, n') \in \mathbb{Z}^2 \times \mathbb{N}, B_K(x, n) \subset B_K(y, n') \subset X \Rightarrow (x, n) = (y, n')$.
For $K = P$, it is well known that the (K, K)-median axis corresponds to the union of the centers of maximal K-balls [5]. We are going to prove that the $(4, 8)$-median axis corresponds to the union of the centers of maximal $(4, 8)$-*fuzzy balls* (see Figure 4), which are recursively defined as follows:

(1) A $(4, 8)$-fuzzy ball of radius 1 and center x $B_{(4,8)}(x, 1)$ is any set verifying: $B_4(x, 1) \subset B_{(4,8)}(x, 1) \subset B_8(x, 1)$.
(2) A $(4, 8)$-fuzzy ball of radius n+1 and center x is a set such that there exists F_n^x, a $(4, 8)$-fuzzy ball of center x and radius n such that: $B_{(4,8)}(x, n + 1) = \bigcup_{y \in F_n^x} B_{K_y}(y, 1)$, where K_y is 4 or 8, depending on y.

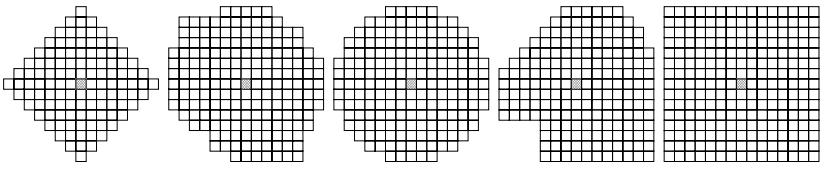

Fig. 4. Some $(4, 8)$-fuzzy balls of radius 7. The extremal cases of $(4, 8)$-fuzzy balls are respectively the 4-ball (on the left), and the 8-ball (on the right).

To prove the identity between the $(4, 8)$-median axis and the locus of the centers of maximal $(4, 8)$-fuzzy balls, we need to use the morphological erosion and dilation:
Let $b \in \mathbb{Z}^2$. The *translated* of X by b is the set $X_b = \{x + b; x \in X\}$.
Let $B \subset \mathbb{Z}^2$. The *morphological dilation* of X by B is defined as:

$$X \oplus B = \bigcup_{b \in B} X_{-b} = \{z \in \mathbb{Z}^2; B_z \cap X \neq \emptyset\}$$

The *morphological erosion* of X by B is defined as:

$$X \ominus B = \bigcap_{b \in B} X_{-b} = \{z \in \mathbb{Z}^2; B_z \subset X\}$$

We also need to prove the following lemma:

Lemma 1 *If $B_{(4,8)}(x,n)$ is a $(4,8)$-fuzzy ball of radius n and center x, and if $y \in B_8(x,1)$, then $[B_{(4,8)}(x,n) \cup B_4(y,n+1)]$ is a $(4,8)$-fuzzy ball of radius $n+1$ and center y.*

Preliminary remark: it is clear, by the definition of fuzzy balls, that if F_n^x is a $(4,8)$-fuzzy ball of center x and radius n, then any set S verifying:

$$F_n^x \oplus B_4(0,1) \subset S \subset F_n^x \oplus B_8(0,1) \tag{1}$$

is a $(4,8)$-fuzzy ball of center x and radius $n+1$. Now we prove the lemma by induction on n. If $n = 0$, $B_{(4,8)}(x,0) = \{x\}$. If $y \in B_8(x,1)$, $B_4(y,1) \subset \{x\} \cup B_4(y,1) \subset B_8(y,1)$, so $[B_{(4,8)}(x,0) \cup B_4(y,1)]$ is a $(4,8)$-fuzzy ball of radius 1 and center y.
Now suppose the lemma true for radii less than or equal to $(n-1)$. Let $B_{(4,8)}(x,n)$ be a $(4,8)$-fuzzy ball of radius n and center x. By definition, there exists F_{n-1}^x, a $(4,8)$-fuzzy ball of center x and radius $(n-1)$ such that:

$$B_{(4,8)}(x,n) = \bigcup_{z \in F_{n-1}^x} B_{K_z}(y,1) \tag{2}$$

and

$$F_{n-1}^x \oplus B_4(0,1) \subset B_{(4,8)}(x,n) \subset F_{n-1}^x \oplus B_8(0,1) \tag{3}$$

Let $y \in B_8(x,1)$. By induction hypothesis, $G_n^y = F_{n-1}^x \cup B_4(y,n)$ is a $(4,8)$-fuzzy ball of radius n and center y.

$$\begin{aligned} G_n^y \oplus B_4(0,1) &= (F_{n-1}^x \oplus B_4(0,1)) \cup (B_4(y,n) \oplus B_4(0,1)) &(4)\\ &= (F_{n-1}^x \oplus B_4(0,1)) \cup B_4(y,n+1) &(5)\end{aligned}$$

So, from (3), we get:

$$G_n^y \oplus B_4(0,1) \subset [B_{(4,8)}(x,n) \cup B_4(y,n+1)] \tag{6}$$

On the other hand, we have:

$$G_n^y \oplus B_8(0,1) = (F_{n-1}^x \oplus B_8(0,1)) \cup (B_4(y,n) \oplus B_8(0,1)) \tag{7}$$

and as

$$B_4(y, n+1) \subset (B_4(y, n) \oplus B_8(0, 1)) \tag{8}$$

from (3), we get:

$$[B_{(4,8)}(x, n) \cup B_4(y, n+1)] \subset G_n^y \oplus B_8(0, 1) \tag{9}$$

Finally, as G_n^y is a $(4, 8)$-fuzzy ball of radius n and center y, we conclude thanks to (6) and (9) that $[B_{(4,8)}(x, n) \cup B_4(y, n+1)]$ is a $(4, 8)$-fuzzy ball of radius $(n+1)$ and center y.

□

Theorem 1 *$S_{(4,8)}(X)$ is the locus of the centers of maximal $(4, 8)$-fuzzy balls in X.*

(1) Right inclusion. Let x be the center of a $(4, 8)$-fuzzy balls $B_{(4,8)}(x, n)$ that is maximal in X. Now suppose that there exists $y \in (B_8(x, 1) \cap X)$ such that $d_4(y, X^c) > d_4(x, X^c)$. Then we must have $B_4(y, n+1) \subset X$. And so:

$$[B_{(4,8)}(x, n) \cup B_4(y, n+1)] \subset X \tag{10}$$

But from lemma 1, $[B_{(4,8)}(x, n) \cup B_4(y, n+1)]$ is a $(4, 8)$-fuzzy ball of radius $n+1$ (see Figure 5(1)), which is in contradiction with the maximality of $B_{(4,8)}(x, n)$.

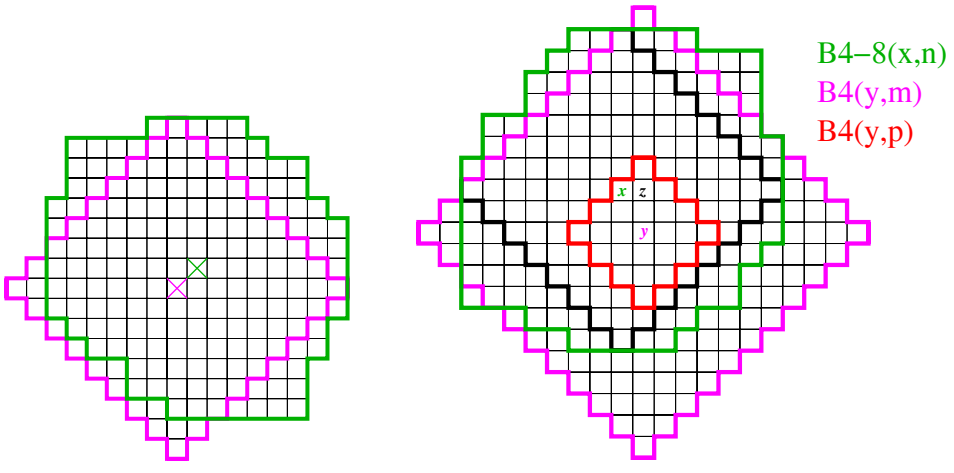

(1) (2)

Fig. 5. (1) The center of a maximal $(4, 8)$-fuzzy ball is an element of $S_{(4,8)}(X)$. (2) An element of $S_{(4,8)}(X)$ is center of a maximal $(4, 8)$-fuzzy ball.

(2) Left inclusion. Let $x \in S_{(4,8)}(X)$. Let $B_{(4,8)}(x,n)$ be the biggest $(4,8)$-fuzzy ball of center x contained in X. We are going to prove that $B_{(4,8)}(x,n)$ is maximal in X.
Suppose that there exists a $(4,8)$-fuzzy ball F_m^y of center y and radius m such that $(y,m) \neq (x,n)$ and $B_{(4,8)}(x,n) \subset F_m^y \subset X$. We have:

$$B_4(y,m) \subset F_m^y \tag{11}$$
$$B_4(x,n) \subset B_{(4,8)}(x,n) \tag{12}$$

The erosion of the ball $B_4(y,m)$ by $B_4(0,n)$ is a ball $B_4(y,p)$ containing x. But $x \notin B_4(y,p) \ominus B_4(0,1)$, otherwise it would mean that $B_4(x,n+1) \subset F_m^y \subset X$, and then $B_{(4,8)}(x,n) \cup B_4(x,n+1)$ would be a $(4,8)$-fuzzy ball of center x and radius $(n+1)$ (see lemma 1) contained in X, which is in contradiction with the fact that $B_{(4,8)}(x,n)$ is the biggest $(4,8)$-fuzzy ball of center x contained in X.
So there must exist $z \in B_4(x,1)$ (see Figure 5(2)) such that $z \in B_4(y,p) \ominus B_4(0,1)$. Then $B_4(z,n+1) \subset F_m^y \subset X$, and so $d_4(z,X^c) > d_4(x,X^c)$. As $z \in B_4(x,1)$, we get $x \notin S_{(4,8)}(X)$, which is in contradiction with our hypothesis.

□

We have now identified the relation between the mixed median axis $S_{(4,8)}(X)$ and a particular class of sets, the $(4,8)$-fuzzy balls. These balls are a new shape description tool, which interest lies in the robustness of morphological or connected skeletons defined in the square grid, as we shall illustrate in the following section.

3 Consequences on the geometrical behavior of MB

The fact that the MB-2 algorithms do not distinguish different $(4,8)$-fuzzy balls (Figure 6(1)), make them more robust with respect to noise (Figure 6(2)), and rotation (Figure 6(3)). Obviously, the outcome is that only partial re-constructibility is possible, unlike MBfp1-8, that allows exact re-constructibility (Figure 6(4), re-constructibility is performed over the skeleton weighted with the distance to the border, with d_4 balls for MBfp1-8, and octagonal balls as a median choice of $(4,8)$-fuzzy balls for MBfp2-8).
Nevertheless, the better behavior of the MB-2 algorithms with respect to rotation is limited to the fact that fewer branches are generated (Figure 6(3)), but if the number of branches is fairly stable for MB-2 on the different rotated versions, their relative positions can vary significantly: see for example Figure 7, and the changes in the hierarchy of the branches. This bias is due to the different errors of the underlying distances (d_4 or d_8 for the fully parallel or

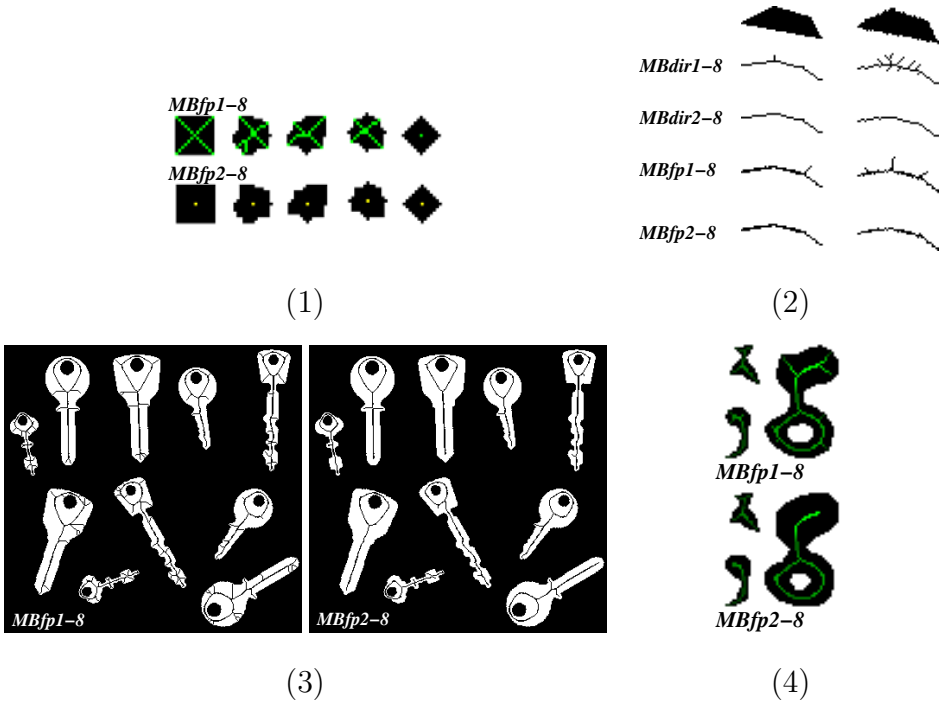

Fig. 6. (1) Some $(4,8)$-fuzzy balls of radius 7 (2) noise immunity (3) rotation invariance (4) re-constructibility.

directional algorithms, respectively) with respect to the Euclidean distance, depending on the angles of the objects.

A first basic idea to get a "more Euclidean" geometry for the skeleton is to

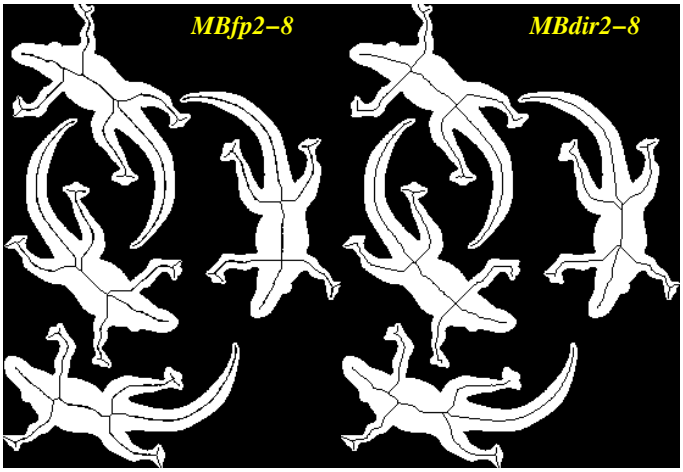

Fig. 7. Limitations of the rotation invariance shown on the image *lizard* at scale 2: the radius of the biggest d_4 (resp. d_8) ball is $\rho = 27$ (resp. $r = 19$).

alternate fully parallel and directional iterations. For example the MB *hybrid* algorithms are defined by Σ-Δ modulation of directional or fully parallel iterations as follows: starting from $S_0 = 0$, at iteration $n > 0$, if $|S_{n-1}+\sqrt{2}/2-n| < |S_{n-1}+\sqrt{2}-n|$, do $S_n = S_{n-1}+\sqrt{2}/2$ and perform one fully parallel iteration, else do $S_n = S_{n-1}+\sqrt{2}$ and perform four directional iterations. By

construction, it turns out that the underlying metrics of the MB hybrid thinning algorithms is generated by the octagonal discrete balls minimizing the maximal error with respect to the Euclidean distance (see an example of such "optimal" octagonal ball on Figure 8). MBhyb1 and MBhyb2 are shown on the last row of Figure 2. This method leads to a significant improvement (compare images of Figure 7 with image at scale 2 of Figure 8), but the bias with respect to Euclidean distance keeps increasing with scale.

Another interesting property of the fuzzy metrics of the MB-2 algorithms

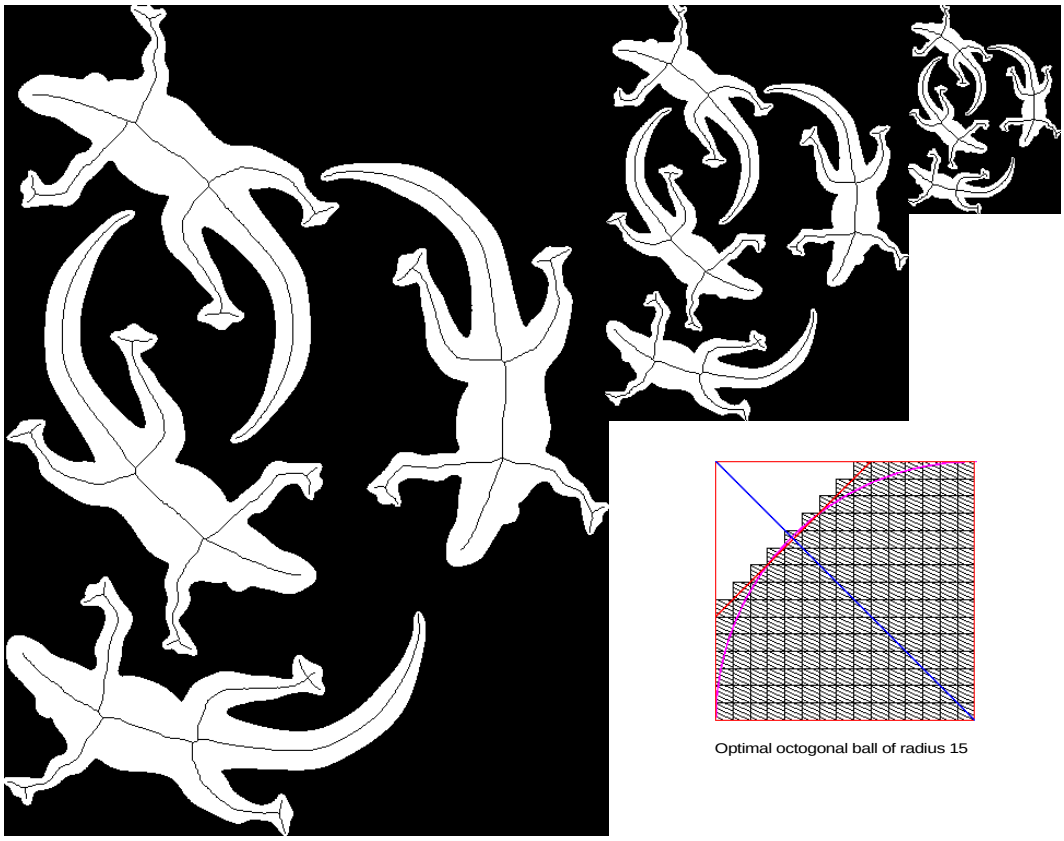

Fig. 8. The MB hybrid skeleton shown on image *lizard* at scales 1, 2 and 3: the radius of the biggest optimal octagonal ball is respectively 41, 21 and 11.

is their ability to be conditioned by a Euclidean or pseudo-Euclidean preprocessed distance. For example, in Figure 9, a chamfer distance transform of support 5 [2] is computed, and then the thinning algorithms are applied by imposing that the pixels deleted at the same iteration are at the same distance to the border. The difference of behaviors between MB-1 and MB-2 shown on Figure 9, and the good invariance to rotation that shows MB2 in that case is explained by the fact that *Euclidean discrete balls are* $(4, 8)$*-fuzzy balls*. So in the case of images where the maximal fuzzy balls are Euclidean, a quasi Euclidean skeleton can be obtained by conditioning MB-2 by the corresponding distance.

The limitation of conditioning lies in the fact that *the set of all* $(4, 8)$*-fuzzy*

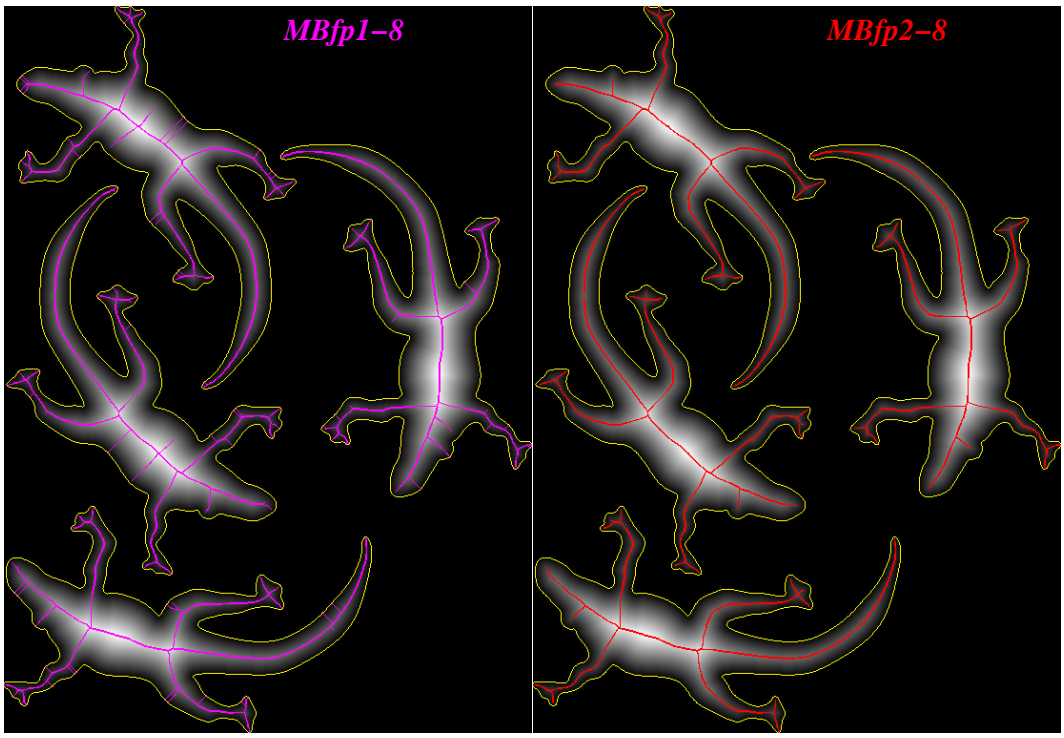

Fig. 9. Conditioning the MB thinning algorithms by a distance transform.

balls is not stable by arbitrary rotation, and this lead to important biases in case of big non Euclidean $(4, 8)$-fuzzy balls (big 4-balls or 8-balls, typically), so for shapes with large perpendicular straight contours.

4 Conclusion

We have shown in this paper the consistency in terms of metrical properties of the family of thinning algorithms we have recently proposed. The geometrical behavior, the advantages and limitations of every algorithm have been clearly identified.
We have shown in [7] that the 8-connected MBfp algorithms could be naturally expressed in the n-dimensional cubic grid, and we have proved the validity of the corresponding algorithms for $n = 3$. The same extension can be done for the other algorithms, but their validity remains to prove. This will be the subject of future work, in order to get hopefully a unified and cleanly justified thinning methodology for n-dimensional binary images.

References

[1] G. Bertrand. On P-simple points. *Comptes Rendus à l'Académie des Sciences*, 321-1:1077–1084, 1995.

[2] G. Borgefors. Distance transformations in digital images. *Computer Vision, Graphics and Image Processing*, vol. 34, 344–371, 1986.

[3] U. Eckhardt and G. Maderlechner. Invariant thinning. *International Journal of Pattern Recognition and Artificial Intelligence*, 7-5:1115–1144, 1993.

[4] A.X. Falcão, L. da Fontoura Costa and B.S. da Cunha. Multiscale skeletons by image foresting transform and its application to neuromorphometry. *Pattern recognition*, vol. 35, 1571–1582, 2002.

[5] C. Lantuéjoul. La squelettisation et son application aux mesures topologiques des mosaïques polycristallines. PhD thesis, Ecole Nationale Supérieure des Mines de Paris, 1978.

[6] L.J. Latecki, U. Eckhardt, and A. Rosenfeld. Well-composed sets. *Computer Vision and Image Understanding*, 61-1:70–83, 1995.

[7] A. Manzanera, T.M. Bernard, F. Prêteux, and B. Longuet. nD skeletonization: a unified mathematical framework. *Journal of Electronic Imaging*, vol. 11(1), 25–37, 2002.

[8] A. Manzanera and T.M. Bernard. MB: A coherent collection of 2D parallel thinning algorithms. *ENSTA/LEI Technical report* LEI/AVA-02-002, 2002. *available at:* http://www.ensta.fr/~manzaner/publis.html/

[9] K. Siddiqi, S. Bouix, A. Tannenbaum and S.W. Zucker. Hamilton-Jacobi skeletons. *International Journal on Computer Vision*, vol. 48(3), 215–231, Kluwer Academic pub., 2002.